Multiscale modeling of thermomechanical behavior of shape memory alloy / polymer composites by finite element method

R. XU[a,b], C. BOUBY[c,d], H. ZAHROUNI[b], T. BEN ZINEB[c,d], H. HU[a], M. POTIER-FERRY[b]

a. School of Civil Engineering, Wuhan University, 8 South Road of East Lake, Wuchang, 430072 Wuhan, PR China rui.xu@whu.edu.cn

b. Laboratoire d'Etude des Microstructures et de Mécanique des Matériaux, LEM3, UMR CNRS 7239, Université de Lorraine, Ile du Saulcy, 57045 Metz Cedex 01, France

c. Université de Lorraine, LEMTA, UMR 7563, Vandoeuvre-lès-Nancy, France

d. CNRS, LEMTA, UMR 7563, Vandoeuvre-lès-Nancy, France

Résumé :

Les matériaux hybrides à comportement multi-physique doivent être étudiés pour contribuer à l'émergence d'applications innovantes tirant profit des propriétés intéressantes des éléments constitutifs en alliages à mémoire de forme (AMF) et en polymères. Les composites fibre-matrice ou multicouches AMF-Polymères pourraient ainsi aboutir à des applications en récupération et conversion d'énergie ou en capteurs-actionneurs. Il est donc important de disposer d'outils numériques de prédiction du comportement non linéaire multi-physique et multi-échelle de ces matériaux. Nous proposons un outil numérique de modélisation du comportement des matériaux composites AMF / Polymères basé sur la méthode des éléments finis multi-échelle. Il s'agit d'une approche numérique itérative dans laquelle les structures macroscopique et microscopique sont discrétisées par éléments finis ce qui permet de traiter les hétérogénéités et les comportements complexes des différentes phases. Le comportement de la phase AMF est décrit par une loi basée sur une approche thermodynamique, dans laquelle les forces motrices associées aux variables internes (fraction volumique de martensite et déformation de transformation moyenne) sont issues du postulat de l'énergie libre de Gibbs. Le comportement du polymère est supposé élastique linéaire et isotrope. La procédure est implantée dans le code d'éléments finis Abaqus via la routine UMAT. L'état de contraintes, la fraction volumique de martensite, ainsi que les opérateurs tangents correspondants sont ainsi calculés et considérés comme entrés au niveau de chaque point d'intégration du maillage de la structure pour le calcul de l'équilibre global. Cette approche multi-échelle est validée sur des cas tests de la littérature. Elle sera par la suite utilisée pour le dimensionnement d'une application en composite AMF / polymère.

Abstract :

Hybrid materials with multi-physical behavior could be developed to contribute to the emergence of innovative applications taking advantage of the interesting properties of shape memory alloys (SMAs) and polymer components. The fiber-matrix or multilayer composites SMA-Polymer could result in applications in energy harvesting or in sensor-actuators. It is therefore important to have numerical tools for predicting the non-linear multi-physical and multi-scale behavior of these composites. In this paper, we propose a numerical tool for modeling the behavior of SMA / Polymer composites based on the multiscale finite element method. It is an iterative numerical approach where the macro and microstructures are discretized by finite element allowing to deal with complex heterogeneities and behaviors of different phases. The behavior of the SMA phase is described by a thermodynamic approach. The driving forces associated with the internal variables (martensitic volume fraction and mean transformation strain) are derived from the postulate of Gibbs free energy. The behavior of the polymer is assumed to be elastic, linear and isotropic. The procedure is implemented in ABAQUS finite element code via UMAT routine. The stress state, volume fraction of martensite, and the corresponding tangent operators are thus calculated and considered as inputs at each integration point of the mesh of the macro-structure for the calculation of the global equilibrium. This multi-scale approach is validated on some test cases of literature. It will subsequently be applied for the designing of a composite SMA / Polymer application.

Mots clefs : Shape memory alloys; Composites; Numerical homogenization; Finite elements.

1 Introduction

Shape memory alloys (*SMAs*) have a wide range of applications such as in aircraft, spacecraft, robotics and medicine fields benefiting from superelasticity and shape memory effects [1,2,3]. Recently, hybrid materials with multi-physical behavior show features in the energy harvesting or in sensor-actuators taking advantages of *SMAs*' superelasticity and shape memory effects. This kind of composites, such as fiber matrix and multilayer composites *SMA*-Polymers, could be developed for innovative applications by taking advantage of the properties of shape memory alloys and polymer components. The response of composites at the macroscopic level and the effective mechanical behavior of the microscopic level is highly related to each other considering the effect of macroscopic factors, such as the thermomechanical loading path, the boundary effect of the macrostructure, and the non-linear and multi-physical behavior of microstructure. It is therefore important to develop a reliable and efficient numerical tools to model the multi-physical, multi-scale and non-linear behavior of these composites.

During the past decades, various existing multiscale methods have been intensively developed for the prediction of mechanical constitutive law of composites. Nezamabadi et al. [4] analyzed the relationship between macroscopic and microscopic instability using *the finite element square (FE²)* method [5,6,7] based on the computational homogenization theory. The FE^2 method achieved the bi-directional real-time transmission of macroscopic and microscopic information by "the macroscopic level transmits the strain to the microscopic *representative volume element* (*RVE*) and the *RVE* transmits the stress to the macroscopic level". In recent years, the FE^2 method has been applied in elastoplastic problem [8], damping [9], heterogeneous shells [10] and *SMA* fiber composites [11]. Inspired by the predecessors' work, this technique is adopted in our proposed numerical tool for modeling the effective behavior of *SMA* / Polymer composites.

In microscopic scale the behavior of *SMA* is described by a model (see Chemisky et al. [12], Duval et al. [13], Armattoe et al. [14]) based on a thermodynamic approach where the driving forces associated with the internal variables martensitic volume fraction and mean transformation strain, are derived from the postulate of Gibbs free energy. Both a path-dependent transformation strain and a strain mechanism related to twin accommodation are taken into consideration in the formulation of the Gibbs free energy expression. In addition, the effect of tension-compression asymmetry of the transformation strain magnitude, the internal loop, hysteresis and transformation saturation are also considered in this *SMA* behavior model. The behavior of the polymer is assumed to be elastic linear and isotropic at the beginning. It will be possible in a future development to take into account the elastic anisotropy and the viscoelasticity of these polymers. This multi-scale approach is validated on some test cases in the literature. It will subsequently be applied for the designing of a composite *SMA* / Polymer applications.

In order to predict the constitutive law or optimize the characteristics of composite materials, models taking into account the microstructure specifications, such as morphology and the constituent's properties, have been developed. However, these multiscale methods such as numerical homogenization still remain difficult to be adopted by the industries since they are still developed as in-house or "academic" codes and their range of application remains generally small because of the need of important implementation effort. To overcome this limitation, developing the multiscale method on the basis of commercial software which is convenient and stable for the users, such as ABAQUS, is a relatively effective choice [15]. Therefore, both a macroscopic model and a microscopic model are built in ABAQUS and are coupled via the *user-defined subroutine* (*UMAT*). The strain components of the integration points are calculated in the macroscopic model discretized by finite element method and is applied on the boundary of the associated *RVE* with *periodic boundary conditions* (*PBC*). The stress-state, volume fraction of martensite, and the corresponding tangent operators are thus calculated in microscopic model and considered as inputs at each integration point for the calculation in macrostructure via *UMAT* routine. The detailed implementation will be illustrated in next section.

2 Methods

2.1 Homogenization

Considering the composite structure is divided into macroscopic and microscopic two levels, a periodic multiphase microscopic structure is assumed to describe the heterogeneity of the material. Two models are implemented in ABAQUS which represent macrostructure and microstructure respectively. In order to distinguish the unknowns of two scales, all the averaged macroscopic values are represented by notation $\bar{(\cdot)}$. In macroscopic model, the unknown constitutive behavior represented by the tangent operator tensor $\bar{\mathbb{C}}_t$ needs to be calculated by a homogenization method in the micro model via *UMAT* routine which is very convenient to implement user-behavior models, while in micro level all the properties and morphology of the different phases are already defined in the process of building the micro model. It is worth to mention that one can have a local constitutive law elastic, thermo-elastic, plastic, viscoplastic or others defined in ABAQUS's material library. When the calculation for macroscopic scale is down, the macroscopic strain $\bar{\boldsymbol{\varepsilon}}$ or its increment $\Delta\bar{\boldsymbol{\varepsilon}}$ at each integration point will be transferred to the associated *RVE* with *periodic boundary conditions* for updating the macro stress $\bar{\boldsymbol{\sigma}}$ or its increment $\Delta\bar{\boldsymbol{\sigma}}$ and tangent constitutive behavior $\bar{\mathbb{C}}_t$.

We assume that the two-dimensional microstructure is a periodic *RVE* with a domain ω and external boundary $\partial\omega$ in its initial configuration (see **Fig. 1**).

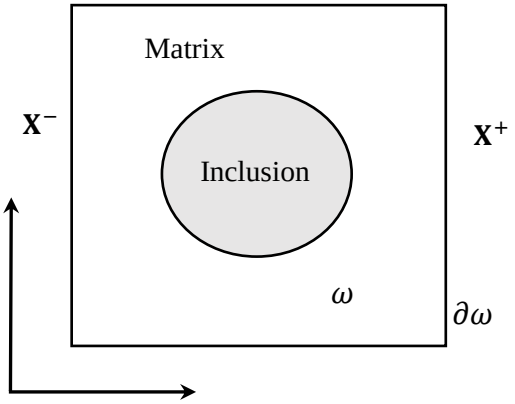

Fig. 1. 2D square *RVE* illustration.

To obtain the effective constitutive law of the heterogeneous 2D *RVE* model, the macroscopic strain at the integration points is applied on the boundary of the corresponding *RVE* with *periodic boundary conditions*:

$$\mathbf{u}^+ - \mathbf{u}^- = \bar{\boldsymbol{\varepsilon}}\,(\mathbf{X}^+ - \mathbf{X}^-) \quad \text{on} \quad \partial\omega, \tag{1}$$

where **u** is the microscopic displacement vector and **X** is the coordinate vector of a given material point at its initial configuration. The exponents + and - represent the nodes on the opposite boundaries of *RVE*. *Periodic boundary conditions* (*PBC)* satisfy the so-called *averaging theorem*, which requests that the average of the work decomposes into the product of work-averages (see Miehe [16]):

$$\frac{1}{|\omega|}\int_{\omega} \boldsymbol{\sigma}\colon\boldsymbol{\varepsilon}\, d\omega - \bar{\boldsymbol{\sigma}}\colon\bar{\boldsymbol{\varepsilon}} = 0, \tag{2}$$

where $\boldsymbol{\sigma}$ and $\boldsymbol{\varepsilon}$ denote the stress and strain tensors at micromodel, $|\omega|$ being the volume of the *RVE*. The behavior of the polymer which can be described by an explicit expression of the constitutive law is given as:

$$\boldsymbol{\sigma} = \mathbb{C}^{(r)}\colon\boldsymbol{\varepsilon}, \tag{3}$$

where $\mathbb{C}$ refers to elastic tensor associated with phase (r). It is worth noting that any other constitutive law can be introduced into the representative volume element, such as *SMAs*' behavior which will be introduced in the following section. The formulation of microscopic visual work is written as:

$$\begin{cases} \displaystyle\int_{\omega} \boldsymbol{\sigma}\colon\delta\boldsymbol{\varepsilon}\, d\omega = 0, \\ \mathbf{u}^+ - \mathbf{u}^- = \bar{\boldsymbol{\varepsilon}}\,(\mathbf{X}^+ - \mathbf{X}^-) \ \text{ on } \ \partial\omega. \end{cases} \tag{4}$$

To impose the deformation at the *RVE*, the superposition principle is used to decompose the strain tensor (considering the symmetry $\bar{\boldsymbol{\varepsilon}}_{12}$=$\bar{\boldsymbol{\varepsilon}}_{21}$) in the following way:

$$\bar{\boldsymbol{\varepsilon}} = \bar{\boldsymbol{\varepsilon}}_{11}\begin{bmatrix}1 & 0\\ 0 & 0\end{bmatrix} + \bar{\boldsymbol{\varepsilon}}_{22}\begin{bmatrix}0 & 0\\ 0 & 1\end{bmatrix} + \bar{\boldsymbol{\varepsilon}}_{12}\begin{bmatrix}0 & 1\\ 1 & 0\end{bmatrix}, \tag{5}$$

which results in the decomposition of equation (1):

$$\mathbf{u}^{(ij)+} - \mathbf{u}^{(ij)-} = \bar{\boldsymbol{\varepsilon}}_{(ij)}\left(\mathbf{X}^{(ij)+} - \mathbf{X}^{(ij)-}\right) \quad \text{on} \quad \partial\omega, \tag{6}$$

where exponents ij $(i,j=1,2)$ denote a set of opposite edges i under strain $\bar{\boldsymbol{\varepsilon}}_{(ij)}$ in direction j. *Periodic boundary conditions* are introduced automatically by the *Equation* function in ABAQUS using python script. With the macroscopic strain $\bar{\boldsymbol{\varepsilon}}$ loaded on the microscopic boundary, we can solve the microscopic problem and calculate the macroscopic stress $\bar{\boldsymbol{\sigma}}$ by:

$$\bar{\boldsymbol{\sigma}} = \frac{1}{\sum_1^N V_m} \sum_1^N V_m \cdot \boldsymbol{\sigma}_m, \tag{7}$$

where V_m denotes the volume associated to the m^{th} integration point. Following equation (1) the strain between the two levels have relation as:

$$\bar{\boldsymbol{\varepsilon}} = \frac{1}{\sum_1^N V_m} \sum_1^N V_m \cdot \boldsymbol{\varepsilon}_m, \tag{8}$$

and $\bar{\boldsymbol{\sigma}}$ and $\bar{\boldsymbol{\varepsilon}}$ are linked by:

$$\partial\bar{\boldsymbol{\sigma}} = \bar{\mathbb{C}}_t : \partial\bar{\boldsymbol{\varepsilon}}. \tag{9}$$

2.2 Nonlinear multilevel procedure

The iterative process between the micro and macro scales is mainly divided into two parts, as shown in **Fig. 2**.

Step 1: Initialization

At the beginning of an increment in the calculation of macro model, we have to obtain the effective constitutive behavior by the homogenization of the micro model. To compute the tangent modulus $\bar{\mathbb{C}}_t$, a unit stain $\bar{\boldsymbol{\varepsilon}}_{(ij)}$ is applied on the boundary of the micro model. This procedure is carried out in the framework of *UMAT* routine using the *Static Linear Perturbation Step object* in ABAQUS:

$$\bar{\boldsymbol{\sigma}} = \bar{\mathbb{C}}_t : \bar{\boldsymbol{\varepsilon}}. \tag{10}$$

Step 2: Convergence analysis

When the macro model got the effective behavior and calculated the macro strain increment $\Delta\bar{\boldsymbol{\varepsilon}}$, *UMAT* will transfer the strain increment $\Delta\bar{\boldsymbol{\varepsilon}}$ at each integration point to the micro model. Then a *Static Step* in ABAQUS is performed in the micro model with the applied strain $\Delta\bar{\boldsymbol{\varepsilon}}$ and the averaged stress $\bar{\boldsymbol{\sigma}}$ at each macroscopic integration point is calculated for checking the convergence of the macro model. The *Static Step* allows the micro model to upgrade its stress and strain state after each calculation. If the convergence analysis of the macro model is not satisfied, a new strain increment $\Delta\bar{\boldsymbol{\varepsilon}}'$ in the current ABAQUS increment will be transferred to the micro model to compute a new stress at the micro level.

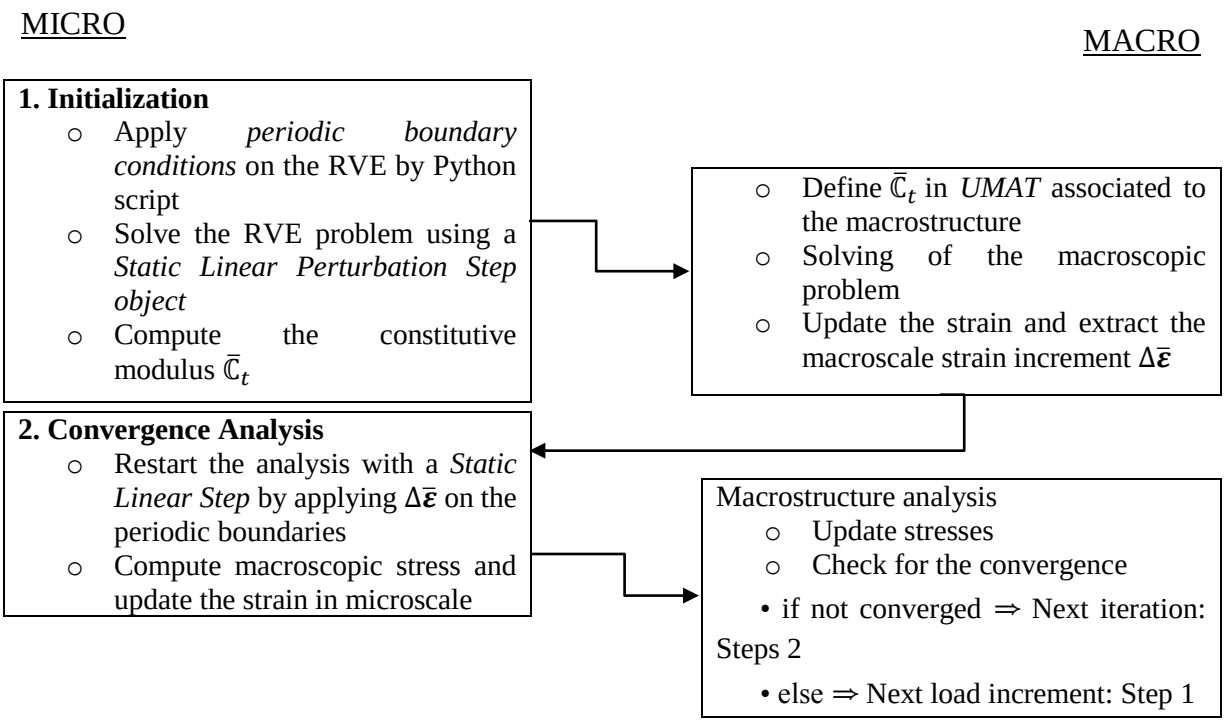

Fig. 2. The nonlinear interactive procedure between the micro and macro models.

2.3 *SMAs* constitutive behavior

As we have mentioned previously that different phases in the micro model can be defined with elastic, thermo-elastic or other mechanical properties in ABAQUS's material library, one can also introduce the user defined *SMA* materials to the micro model by *UMAT*. Here we adopt the constitutive model developed by Chemisky et al. [12] which considered three main physical mechanisms: the martensitic transformation, the reorientation of martensitic and the inelastic accommodation of twins in self-accommodated martensite. Research shows that this model can capture the behavior of *SMA*s even under complex thermomechanical paths, especially when transformation occurs at low stress level.

We assume that behavior of *SMA* is characterized by a *RVE* containing martensitic and austenitic phases. Considering an additive decomposition of strain without plastic or viscoplastic strain, the total strain of the *SMA* is written as:

$$\boldsymbol{\varepsilon} = \boldsymbol{\varepsilon}^e + \boldsymbol{\varepsilon}^{th} + \boldsymbol{\varepsilon}^T + \boldsymbol{\varepsilon}^{twin}, \tag{11}$$

where $\boldsymbol{\varepsilon}^e$ denotes the elastic strain, $\boldsymbol{\varepsilon}^{th}$ denotes the thermal strain, $\boldsymbol{\varepsilon}^T$ represents the inelastic strain due to martensitic transformation and $\boldsymbol{\varepsilon}^{twin}$ refers to the inelastic strain due to the accommodation of twins between martensitic variants.

Assuming both martensitic and austenitic phases are isotropic and have the same thermo-elastic constants, the elastic strain and the strain due to thermal expansion are expressed as:

$$\boldsymbol{\varepsilon}^e = \mathbb{S}:\boldsymbol{\sigma}, \tag{12}$$

$$\boldsymbol{\varepsilon}^{th} = \boldsymbol{\alpha}\left(T - T_{ref}\right), \tag{13}$$

where $\mathbb{S}$ is the isotropic fourth order compliance tensor, $\boldsymbol{\alpha}$ is the isotropic thermal expansion tensor, and T_{ref} is the reference temperature where thermal expansion strain is selected to be null. Transformation strain can be expressed as the average value over the a micro-*RVE* of local transformation strain field:

$$\boldsymbol{\varepsilon}^{T} = f\tilde{\boldsymbol{\varepsilon}}^{T}, \tag{14}$$

where f denotes the average martensitic volume fraction and describes the martensitic transformation, $\tilde{\boldsymbol{\varepsilon}}^{T}$ denotes the mean transformation strain over the martensite volume and describes the reorientation of martensite.

The strain associated to the inelastic accommodation of twins between martensitic variants is written:

$$\boldsymbol{\varepsilon}^{twin} = f^{FA}\tilde{\boldsymbol{\varepsilon}}^{twin}, \tag{15}$$

where f^{FA} denotes the formed self-accommodated martensitic volume fraction and $\tilde{\boldsymbol{\varepsilon}}^{twin}$, denotes the mean twin accommodation strain over the martensitic volume and describes the inelastic accommodation of twins in self-accommodated martensite. With the four presented internal variables f, f^{FA}, $\tilde{\boldsymbol{\varepsilon}}^{T}$, $\tilde{\boldsymbol{\varepsilon}}^{twin}$, we can define the Gibbs free energy potential and deduce the transformation force F_f, orientation force $F_{\tilde{\varepsilon}^T}$
and twin accommodation force $F_{\tilde{\varepsilon}^{tw}}$ with associated criterions for adjusting the loading path. This constitutive model is implemented in the *UMAT* routine of the micro model.

3 Numerical results

3.1 Effective behavior of RVE

In this section, the simulation of several isothermal tension and shear loading paths are performed to study the effective superelastic behavior of the homogenized hybrid *SMA* / polymer composites. Considering a 2D *RVE* made of elastic polymer inclusion and *SMA* matrix as shown in **Fig. 1**, both tension in direction 11 and shear in direction 12 with *PBC* are tested with the mechanical properties listed in Table 1. E_s, ν_s are the Young's modulus and Poisson's ratio respectively for the *SMA* and E_p, ν_p respectively for the polymer. Since the temperature T in the simulations is above the austenitic finish temperature A_f, *SMA* matrix presents a superelastic behavior. The element type CPS3 (2D triangular continuum solid and isoparametric element with linear interpolation and plane stress assumption) is adopted in the fine meshed *RVE* while the volume fraction of the inclusion F_i is 0.3 (see **Fig. 3**). In **Fig. 3**, the nodes on the boundaries are highlighted with circles as a result of the introduction of *PBC* with *Equation* in ABAQUS's *Interaction* module.

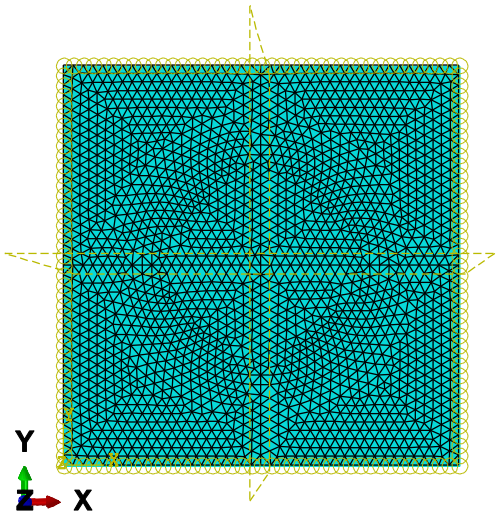

Fig. 3. The fine meshed *RVE* with CPS3 element and the *PBC* on the boundary nodes.

Table 1
Mechanical properties for hybrid *SMA* / polymer composites.

E_p(MPa)	ν_p	F_i	T (°C)	E_s(MPa)	ν_s	M_s(°C)
7000	0.3	0.3	0	70000	0.3	-50
A_f(°C)	α(°C^{-1})	ε^T_{trac}	$\varepsilon^{T\,FA}_{trac}$	ε^T_{comp}	B_f(MPa °C^{-1})	B_r(MPa °C^{-1})
-20	8e-6	0.05	0.04	0.04	5	6
M_s(°C)	A_f(°C)	r_f	F_ε(MPa)	H_f(MPa)	H_{ε^T}(MPa)	H_{twin}(MPa)
-50	-20	0.6	100	4	1000	40000
H_s(MPa)						
50						

For the first case, we assume the matrix is made of *SMA* materials and the inclusion is made of elastic polymer. **Fig. 4** (a) and (c) show the effective behavior of *RVE* in tension test with applied stretch strain intensity up to 2%, 3% and 4% respectively, while **Fig. 4** (b) and (c) show the effective behavior of *RVE* in shear test with applied shear strain intensity up to 2%, 3% and 4% respectively. The *RVE* inherits the superelasticity of the *SMA* components and the loading path is highly related to the loading history (see Chemisky et al. [12]).

The effective stress $\bar{\boldsymbol{\sigma}}$ and strain $\bar{\boldsymbol{\varepsilon}}$ are calculated by the averaging of variables in the whole *RVE* volume using Eqs. (7) and (8). In **Fig. 4** (a), the maximum strains applied on the boundary with *PBC* are 2%, 3% and 4% and the associated averaged strains are 1.94%, 2.94% and 3.9% respectively, with the relative error of the effective strain being controlled in about 2%. In **Fig. 4** (b) the relative error of the effective shear strain is controlled in about 0.03%. We conclude this magnitude of error is small enough to satisfy the *averaging theorem*.

For the second case, same simulations are performed by only swapping the material behaviors of the components of the *RVE* of the first case. As shown in **Fig. 5**, the whole stiffness of the *RVE*, the width of the hysteresis loops and the transformation's effect on the effective stress-strain slope are much smaller than the first case, since the volume fraction of the *SMA* is only 0.3. At the beginning of the reverse transformation in **Fig. 5** (c) and (d), the averaged martensitic volume fraction varies much quicker than in

Fig. 4 (c) and (d). This is because of the phase transformation in the second case is almost synchronous but in the first case are not, as a result of the difference of the stresses distributed in the matrix.

The internal loops are observed in the partial loops of both the first and the second cases. During the forward transformation, the stress-strain loading paths are coincided while during the reverse transformation, the occurrence of the reverse transformation is dependent on the current martensitic transformation $\bar{f}$ (see Chemisky [12]). As the inclusion is elastic in the first case, the stress-strain slope in the partial loop varies slower than for the pure *SMA* materials, but the *RVE* still shows obvious hysteresis related to the phase transformation. When the applied strain vanishes during the reverse transformation, stress in the *RVE* is not vanishing because the reverse transformation is not complete and the martensitic volume fraction is not equal to 0.

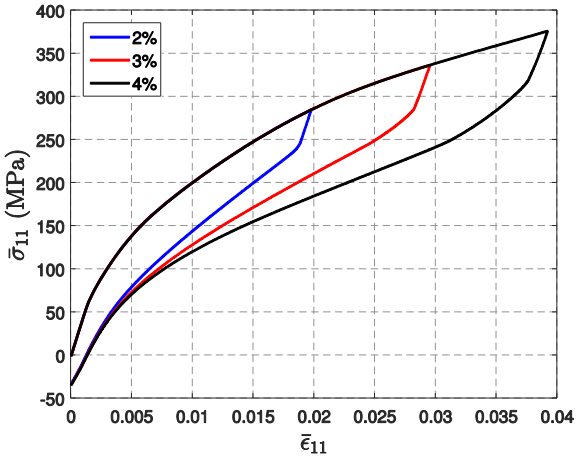

(a) The effective stress-strain behavior of *RVE* in tension test with applied strain intensity up to 2%, 3% and 4% respectively.

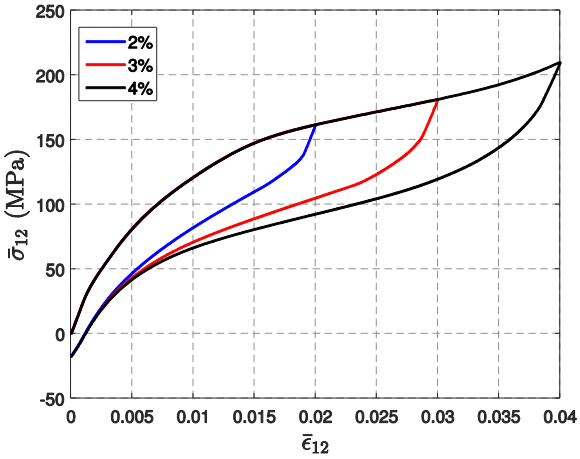

(b) The effective stress-strain behavior of *RVE* in shear test with applied strain intensity up to 2%, 3% and 4% respectively.

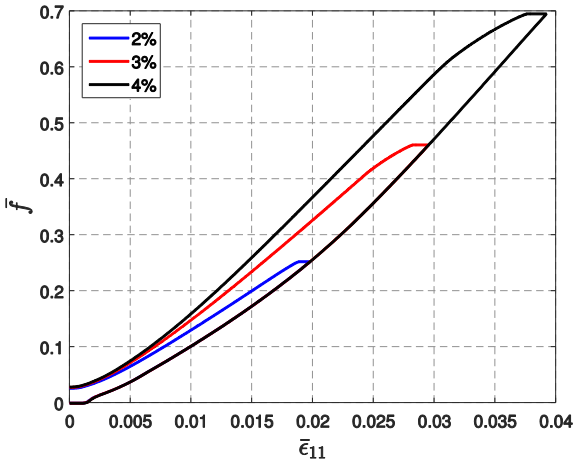

(c) Averaged martensitic volume fraction $\bar{f}$ versus strain associated with **Fig. 4** (a).

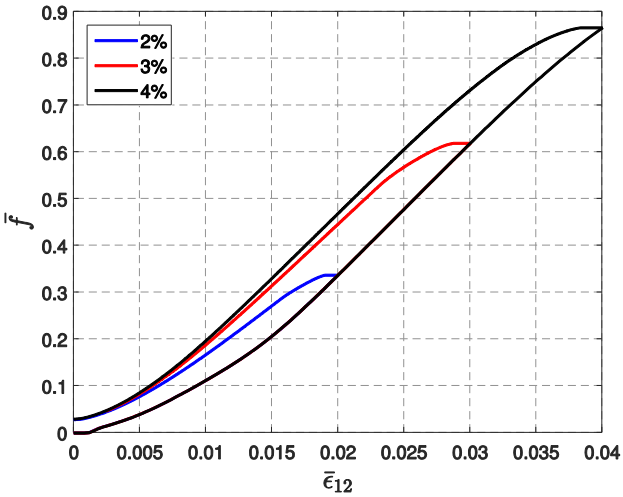

(d) Averaged martensitic volume fraction $\bar{f}$ versus strain associated with **Fig. 4** (b).

Fig. 4. Isothermal tension and shear loading tests for *SMA* matrix and elastic inclusion *RVE*.

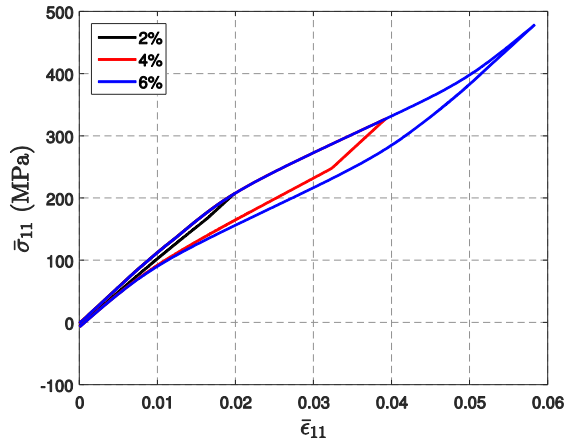

(a) The effective stress-strain behavior of *RVE* in tension test with applied strain intensity up to 2%, 4% and 6% respectively.

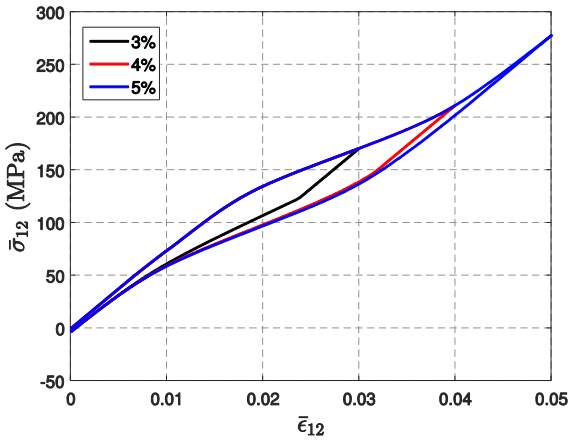

(b) The effective stress-strain behavior of *RVE* in shear test with applied strain intensity up to 3%, 4% and 5%, respectively.

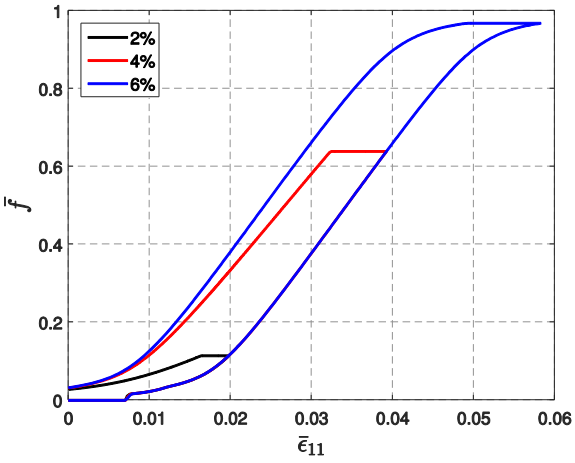

(c) Averaged martensitic volume fraction $\bar{f}$ versus strain associated with **Fig. 5** (a).

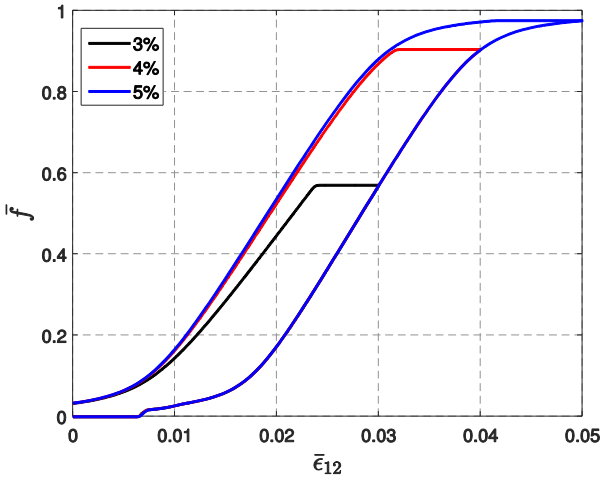

(d) Averaged martensitic volume fraction $\bar{f}$ versus strain associated with **Fig. 5** (b).

Fig. 5. Isothermal tension and shear loading tests for *SMA* inclusion and elastic matrix *RVE*.

3.2 Bending test

As shown in **Fig. 6**, an elastic cantilever beam subjected to a concentrated load P is used to get a reliable loading history of a bending case, with Young's modulus E_{beam}=7000MPa, ν_{beam}=0.3 (corresponding to the elastic behavior of the polymer) and P = 50N. The strains and step times of point A are extracted during the loading history and applied on the boundary of the microscopic *RVE* model. For this case the

volume fraction of the inclusion is set to 0.3, while other properties remain the same as the previous section.

With this loading conditions, the obtained stress versus strain diagram of two main directions 11 and 12 are illustrated in the **Fig**. **7**. Like the tests of the *RVE* under pure traction or shear deformation, the hysteresis behavior is captured in **Fig. 7** (a) when the maximum strain $\bar{\varepsilon}_{11}$ is up to 0.05. During the loading process, the stress-strain slope becomes smaller when the averaged strain $\bar{\varepsilon}_{11}$ reaches 0.02, since the increase of the averaged martensitic volume fraction $\bar{f}$ is fast with the increase of $\bar{\varepsilon}_{11}$**.** After strain $\bar{\varepsilon}_{11}$ reaches 0.04, the slope of the averaged martensitic volume fraction $\bar{f}$ versus strain $\bar{\varepsilon}_{11}$ diagram decreases, see **Fig. 7** (c), because the transformation process has almost reached saturation in some area of the inclusion. During the reverse transformation process, the austenitic volume fraction quickly generates when strain $\bar{\varepsilon}_{11}$ reaches 0.035 as shown in **Fig. 7** (c), which results in the change of the slope of the effective stress-strain diagram. When the strain $\bar{\varepsilon}_{11}$ reaches 0.01, the reverse transformation is almost finished and the slope of the unloading path in **Fig. 7** (a) is constantly close to the slope when the loading loop begins. Finally, the hysteresis effect due to the transformation of the *SMA* inclusion is observed in **Fig. 7** (a). In **Fig. 7** (b). Similar hysteresis effect of the stress-strain diagram in direction 12 is also simulated. During the forward transformation, the effect of the transformation to the slope of the stress-strain diagram is not as obvious as the effect in direction 11. When the strain $\bar{\varepsilon}_{12}$ decreases to 0.015, the reverse transformation in most area of the *SMA* inclusion begins which leads to the change of the slope in **Fig. 7** (b). At last the averaged stress in the *RVE* does not completely vanish because the reverse transformation is not complete and the martensitic volume fraction is not equal to 0. In general, these results show that the homogenized micro model made of *SMA* inclusion and polymer matrix is able to simulate the transformation behavior and hysteresis during the loading loops for bending test.

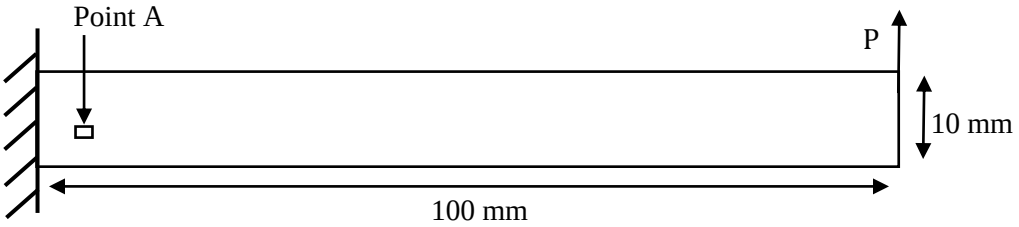

Fig. 6. Elastic cantilever beam subjected to a concentrated load.

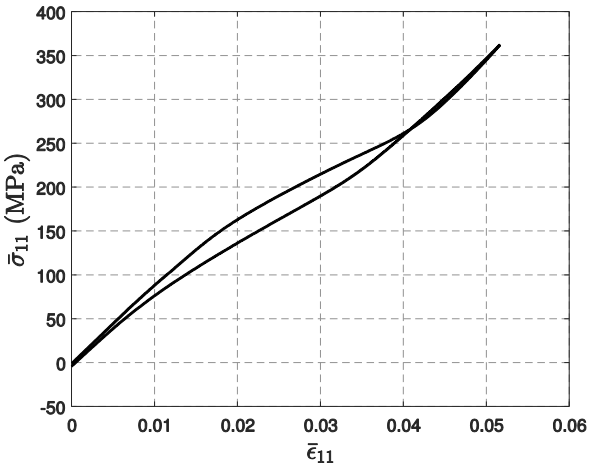

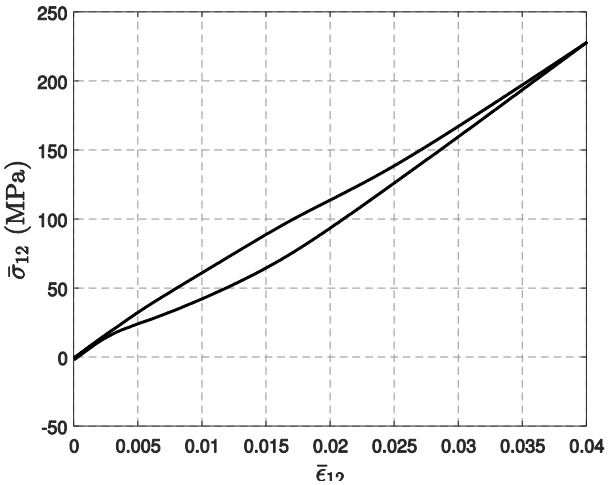

(a) The effective stress-strain behavior in direction 11.

(b) The effective stress-strain behavior in direction 12.

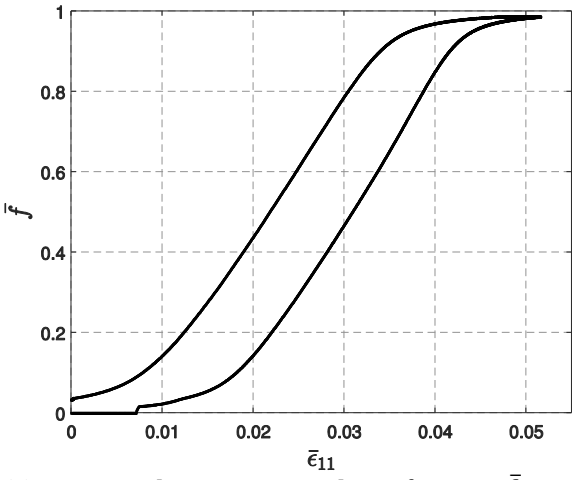

(c) Averaged martensitic volume fraction $\bar{f}$ versus strain $\bar{\varepsilon}_{11}$ diagram.

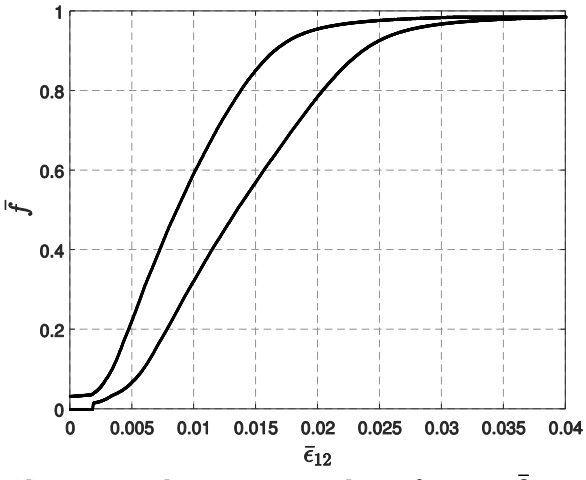

(d) Averaged martensitic volume fraction $\bar{f}$ versus strain $\bar{\varepsilon}_{12}$ diagram.

Fig. 7. Bending test for *SMA* inclusion and elastic matrix *RVE*.

4 Conclusion

Based on the study of above tests, the effective behavior of the *SMA* / polymer composites shows the characteristics of superelasticity and its influence by the elastic behavior of the polymer. As the combination of the homogenization method and *SMA* model shows good stability, in the next step we will introduce the homogenized *RVE* model to the FE^2 procedure implanted in ABAQUS.

Acknowledgment

This work has been supported by the National Natural Science Foundation of China (Grant No. 11372231), the Science and Technology Agency of Hubei Province (Grant No. 2011CDA047). The authors also gratefully acknowledge the financial support of the French National Research Agency ANR (LabEx DAMAS, Grant No. ANR-11-LABX-0008-01).

Références

[1] Leclercq S., Lexcellent C., 1996. A general macroscopic description of the thermo- mechanical behavior of shape memory alloys. Journal of the Mechanics and Physics of Solids 44, 953-980.
[2] Lagoudas D.C., Entchev P.B., 2004. Modeling of transformation-induced plasticity and its effect on the behavior of porous shape memory alloys. Mechanics of Materials 36, 865-892.

[3] Cisse C., Zaki W., Ben-Zineb T., 2016. A review of modeling techniques for advanced effects in shape memory alloy behavior. Smart Materials and Structures 25, 103001-103036.
[4] Nezamabadi S., Potier-Ferry M., Zahrouni H., Yvonnet J., 2015. Compressive failure of composites: A computational homogenization approach. Composite Structures 127, 60-68.
[5] Feyel F., 2003. A multilevel finite element method (FE^2) to describe the response of highly non-linear structures using generalized continua. Computer Methods in Applied Mechanics and Engineering 192, 3233-3244.
[6] Kousnetzova V.G., Geers M.G.D., Brekelmans W.A.M., 2004. Multi-scale second-order computational homogenization of multi-phase materials: a nested finite element solution strategy. Computer Methods in Applied Mechanics and Engineering 193, 5525-5550.
[7] Nezamabadi S., Yvonnet J., Zahrouni H., Potier-Ferry M., 2009. A multilevel computational strategy for handling microscopic and macroscopic instabilities. Computer Methods in Applied Mechanics and Engineering 198, 2099-2110.
[8] Nezamabadi S., Zahrouni H., Yvonnet J., Potier-Ferry M., 2010. A multiscale finite element approach for buckling analysis of elastoplastic long fiber composites. International Journal for Multiscale Computational Engineering 8, 287-301.
[9] Attipou K., Nezamabadi S., Daya E.M., Zahrouni H., 2013. A multiscale approach for the vibration analysis of heterogeneous materials: Application to passive damping. Journal of Sound and Vibration 332,725-739.
[10] Cong Y., Nezamabadi S., Zahrouni H., Yvonnet J., 2015. Multiscale computational homogenization of heterogeneous shells at small strains with extensions to finite displacements and buckling. International Journal for Numerical Methods in Engineering 104, 235-259.
[11] Kohlhaas B., Klinkel S., 2014. An FE^2 model for the analysis of shape memory alloy fiber-composites.Computational Mechanics 55, 421-437.
[12] Chemisky Y., Duval A., Patoor E., Ben-Zineb T., 2011. Constitutive model for shape memory alloys including phase transformation, martensitic reorientation and twins accommodation. Mechanics of Materials 43, 361–376.
[13] Duval A., Haboussi M., Ben-Zineb T., 2011. Modelling of localization and propagation of phase transformation in superelastic SMA by a gradient nonlocal approach. International Journal of Solids and Structures 48, 1879-1893.
[14] Armattoe K.M., Haboussi M., Ben-Zineb T., 2014. A 2D finite element based on a nonlocal constitutive model describing localization and propagation of phase transformation in shape memory alloy thin structures. International Journal of Solids and Structures 51, 1208-1220.
[15] Tchalla A., Belouettar S., Makradi A., Zahrouni H., 2013. An ABAQUS toolbox for multiscale finite element computation. Composites: Part B 52, 323-333.
[16] Miehe C., Schroder J., Becker M., 2002. Computational homogenization analysis in finite elasticity: material and structural instabilities on the micro- and macroscales of periodic composites and their interactions. Computer Methods in Applied Mechanics and Engineering 191, 4971-5005.